UNSYS digital

Journal of Unmanned System Technology

Preliminary Numerical Analysis of The Effects of Rear Fin-Shape on The Oscillating Propulsion Performance

Arie Sukma Jaya[†] and Muljowidodo Kartidjo[†‡]

[†]Center for Unmanned System Studies, Institut Teknonologi Bandung, Indonesia

[‡]Department of Mechanical Engineering, Institut Teknologi Bandung, Bandung, Indonesia

Abstract— Performance of the oscillating fin with different rear shapes has been analyzed in the present work. Preliminary analysis was performed by using numerical simulations on the interaction between fluid and solid model. Involved rear fin-shapes were based on natural forms of caudal fin of fish such as round, truncate, fork and lunate. From the present result, the rear-shapes affect the optimum performance of the fin such as thrust production, represented by cruising speed, and efficiency. The effects determine suitable mission for each rear-shape such as short, medium, or long cruising endurance. Further numerical study on the effect of material elasticity of the fin, represented by cupping shape of the fin, was also performed. The characteristics of cupping shape increases thrust production of the oscillating fin for impulse thrust generator such as round and truncate rear-shapes.

Keywords— numerical analysis, fin, rear fin shape, propulsion, efficiency, cupping.

DOI: 10.21535/just.v7i1.1039

I. INTRODUCTION

IMMERSED objects in water such as aquatic animals, underwater vehicles, and robots move in water by transferring momentum to the water. Reynolds number, reduced frequency and shape of the object are factors that are affecting the momentum transfer [1]. The principle of momentum transfer in water gives a unique characteristic of underwater propulsion.

Generally, locomotion of fish can be divided based on its swimming propulsors, which are Body-Caudal Fin (BCF) and Median-Paired Fin (MPF) [2]. Periodic undulation movement of the BCF type gives a cruising mode of the locomotion, while MPF type provides a maneuvering movement of the fish. Older classification of BCF type based on part of the fish that contributes to thrust generation is *anguilliform*, *subcarangiform*, *carangiform*, *thunniform*, and *ostraciiform* [3]. Most of those types of fish locomotion have been studied extensively.

Corresponding author: M. Kartidjo (e-mail: mwkartidjo@gmail.com)

This paper was submitted on December 1, 2015; revised on December 21, 2015; and accepted on December 26, 2015.

Locomotion studies of fish have been developed to the creation of bio-inspired underwater object such as robotic fish. RoboTuna is one of the earliest robotic fish inspired by tuna fish [4]. Oscillating foils for high efficient thrust has been researched for the robotic fish [5],[6]. Furthermore, higher efficiency of the oscillating foils than the ordinary screw propeller has been examined as marine propulsion [7]. Parametric study and biomimetic on kinematics of the carangiform robotic fish were also have been developed [8],[9].

Research on how thrust generated by the undulating propulsors has also been flourished. Vortex formation was observed on drag-based propulsor by using Defocusing Digital Particle Image Velocimetry (DDPIV) [10]. DPIV was also performed to investigate thrust production of a robotic caudal fin [11]. Fish biomechanics has also been summarized as 16 results of the experimental analyses in order to provide a better construction of the robotic fish [12].

Beside the experimental approaches, numerical simulations have also been widely performed in order to obtain many physical aspects of the undulating propulsion. 3D hydrodynamics analysis has been performed to improve design and flexibility of the biomimetic robotic fish [13]. Vortex reattachment that is enhancing locomotor force at the leading edge of the fish has also been shown by using numerical simulation [14]. Optimization of the anguilliform swimming mode was also has been numerically investigated [15].

Present work is the preliminary analysis of performance evaluation of the BCF propulsor with oscillating fin by using numerical approach. Oscillating fin on the present work represents the drag-based propulsor, which is categorized into impulse (round and truncate) and vortex (fork and lunate) thrust generators [16]. The main objective of the simulations is to investigate the effects of rear fin-shapes on thrust production and efficiency of the oscillating fin. The effect of elasticity of the fin has been investigated by mimicking stiffness and geometry of a rainbow trout in a certain swimming pattern [17]. In the present work, the effects of surface elasticity on fin were represented by the cupping shape of the fin; following finding in [11], that cupping shape could increase thrust production.

Thrust and efficiency by the presence of cupping shape were compared to the flat shape.

II. Numerical Simulation

A. *Simulation models*

Aquatic animals such as fish have fins as thrust propulsors in order to move in water as can be seen in Figure 1. In the present research, the main focus of the analysis was the performance of caudal fin, as the main thrust propulsor, with different rear fin-shapes. Hence, the models of the fins followed the nature forms of the caudal fins.

Simulation models of the oscillating propulsor were generated three-dimensionally. There were fixed and moving parts. Fixed part was a streamlined body that has a two-third of the overall length of the model. Moving part represented the propulsor. The proportion of the fixed and moving parts was following the carangiform type of the BCF propulsion. The rear fin-shapes were selected based on the common shapes in natural aquatic animals, especially fish. The present model of body and fin were made symmetrical in longitudinal and lateral axes and can be seen in Figure 2.

Geometrical parameters of the models can be seen in Table 1. The overall dimension of the model was 0.5 m × 0.14 m × 0.09 m (Mid-section length × maximum height × maximum width). Fixed body geometry was similar for all simulations. The generated force, especially thrust, was integrated from the pressure difference in the fin surface. Hence, in order to properly compare the generated thrust, fins had similar fluid-surface interface area, S. The end-face of the body and front-face of the fins were an ellipse shape with major axis length, a = 0.022 m and minor axis length, b = 0.025 m.

Characteristics length of the fins, L_F, was measured in the mid-section of the lateral axis. In consequence, L_F was the maximum normal distance from the front face of the fin for round and truncates rear fin-shapes, while it was the minimum normal distance for fork and lunate rear fin-shapes. Furthermore, L_F was the reference of the upper and lower rear-vertexes normal distance from the front face of the fins, L_V, in which $L_V = L_F - 0.05$ m for round rear fin-shape and $L_V = L_F + 0.05$ m for fork and lunate rear fin-shape. L_F represented the characteristics length to determine the Reynolds number of the fluid analysis. Due to constant surface area and height of the fins, aspect ratio, AR, of the fins was also made constant.

Table 1 Geometrical parameters of the models

Body	Length, L_B (m)	0.320
	Width, W_B (m)	0.090
	Height, H_B (m)	0.140
Fins	Surface area, S (m^2)	0.037
	Length, L_F (m)	0.180
	Height, H_F (m)	0.150
	Aspect Ratio, AR	0.608

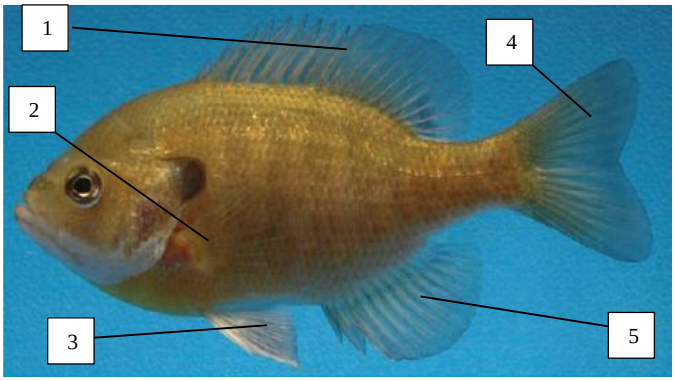

Figure 1 Fins of Bluegill sunfish [11]:
(1) dorsal fin, (2) pectoral fins, (3) pelvic fins, (4) caudal fin, (5) anal fin

Components	Nature Form	Model
Streamline Body	Aquatic animal body	
Round Fin	Shallow water fish Bowfin fish [19] 	
Truncate Fin	Shallow water fish Rainbow trout [20] 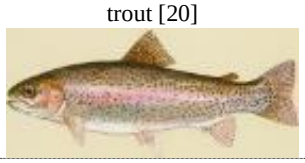	
Fork Fin	Open sea fish Pilot fish [21] 	
Lunate Fin	Oceanic fish Crevalle jack [22] 	

Figure 2 Components of the simulation model

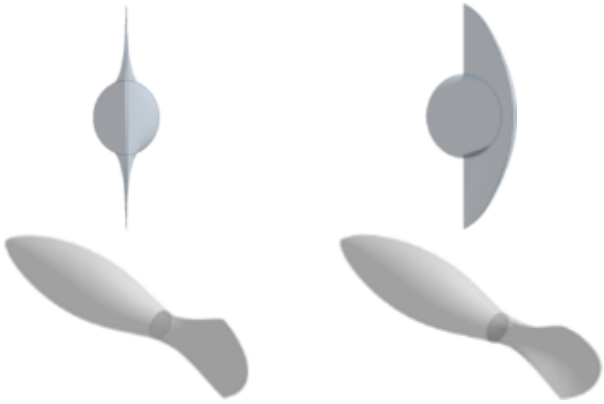

(a) **(b)**

Figure 3 Rear fin-shape curvature: (a) flat, and (b) cupping

Another geometrical aspect of the rear fin-shape in present work was curvature of the rear fin-shape, which were divided into flat and cupping shape, as can be seen in Figure 3(a) and Figure 3(b). Rear curvature of the cupping shape was parameterized by the cupping ratio, C_R, and can be defined as

$$C_R = \frac{c}{H_F} \quad \textbf{(1)}$$

where H_F is the heights of the flat fin and c is the maximum deflection at the mid-section. At the present work, C_R = 0.2 was applied for all cupping simulations. Constant surface area decreased the aspect ratio, AR, of the cupping to AR = 0.493.

The lateral movement, whether flat or cupping type, was a rotational movement at a fixed point relative to the vertical axis of the body. The fixed point was located at the contact faces of the body and propulsor. Double of the tail-beat amplitude, A = 0.125 m and the angular deflection of the propulsor, $\theta = 20^o$.

B. Numerical scheme

Numerical simulations of the present work were performed by using ANSYS Workbench. Coupling between transient structural component and ANSYS-CFX component were involved in the simulations. Oscillation movements of the caudal fin were performed in structural component and the displacements were transferred to the fluid component through *Fluid-Solid Interface* scheme. Computational mesh and mesh properties in the present simulation can be seen in Figure 4 and Table 3 respectively.

The size of computational domain in Error! Reference source not found. was appropriate enough to observe flow phenomena of the model. Water as the fluid was flowing from inlet to outlet. Relative pressure at inlet was set to 0 Pa. The unstructured mesh was generated to accurately capture the flow properties. Inflation layers were implemented in the mesh generation in order to smoothly capture boundary layer on the body and propulsor surfaces.

Number of nodes on the generated mesh was determined by the convergence study. The study consists of five mesh sizing configuration. The relation of number of nodes with performance parameter such as drag and thrust power were performed on round rear fin-shape at flow velocity, V = 0.5 m/s and tail-beat frequency, f = 0.5 s^{-1}. The result of convergence study is tabulated in Table 2. It shows that medium sizing with 90715 nodes is enough accuracy to obtain valuable information with less computational time.

The *k*-omega SST turbulence model was selected as the turbulent model of the present work. This is a two-equation eddy-viscosity model [18]. The turbulence model accounts for the transport of the turbulent shear stress in order to give an accurate prediction of the onset and the amount of flow separation.

Recorded outputs of the simulations in the present work were total force on the body and propulsor and total torque of the propulsor. The term total was the sum of the normal and tangential components of force or moment that were acted in a specified axis. Total forces in similar direction with the fluid flow can be divided into drag, D, in positive direction and thrust, T, in negative direction. Net force, F_{Net}, in the flow direction then

$$F_{Net} = T - D \quad \textbf{(2)}$$

At the balance condition between thrust and drag, F_{Net} = 0 N, cruising speed, V_C, can be approximated.

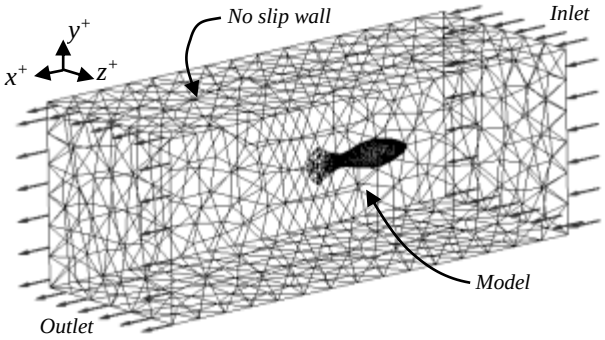

Figure 4 Computational mesh

Table 2 Convergence Study

Mesh Sizing	Number of Nodes	Thrust Power (W)	Lateral Power (W)	Efficiency (%)
Very coarse	60542	0.59	0.66	47.42
Coarse	75025	0.95	0.77	55.15
Medium	90715	1.01	0.79	55.81
Fine	104954	1.02	0.82	55.56
Very fine	120769	1.05	0.82	56.06

Table 3 Numerical Scheme Properties

Numerical analysis	ANSYS MultiField (Transient Structural and ANSYS CFX)
Computational domain Size	Length: 4L, Width: 1.5L, Height: 1.5L (L is overall length of the model)
Mesh type	Unstructured Tetrahedral (90715 Nodes)
Inflation layer	15
Turbulence model	Shear Stress Transport (Automatic Wall Function)
Transient scheme	Second Order Backward Euler
Velocity	0.1 m/s ~ 0.75 m/s
Tail-beat frequency	0.25 s^{-1} ~ 1 s^{-1}
Reynolds number	$5.6 \times 10^4 \sim 2.8 \times 10^5$
Strouhal number	0.0625 ~ 0.625

Thrust power, P_T, drag power, P_D, and lateral power, P_L, can be expressed as

$$P_D = \bar{D} \times V \quad \textbf{(3)}$$

$$P_T = \bar{T} \times V \quad \textbf{(4)}$$

$$P_L = \bar{Q}_Y \times \omega \quad \textbf{(5)}$$

In (5), $\bar{Q}_Y$ is the mean value of the torque in Y-axis and ω is the angular velocity of the propulsor. Therefore, P_L can be considered as the required power to generate thrust. The efficiency of the propulsor, η, can be expressed as

$$\eta = \frac{P_T}{P_T + P_L} \quad \textbf{(6)}$$

Tail-beat frequency (s^{-1})	Velocity (m/s)	Rear fin-shape			
		Round	Truncate	Fork	Lunate
0.5	0.25	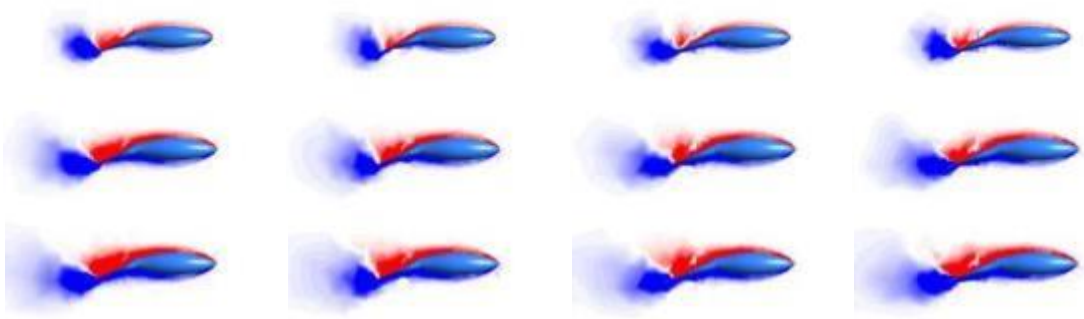			
	0.5				
	0.75				

(a)

Velocity (m/s)	Tail-beat Frequency (s^{-1})	Rear fin-shape			
		Round	Truncate	Fork	Lunate
0.5	0.25	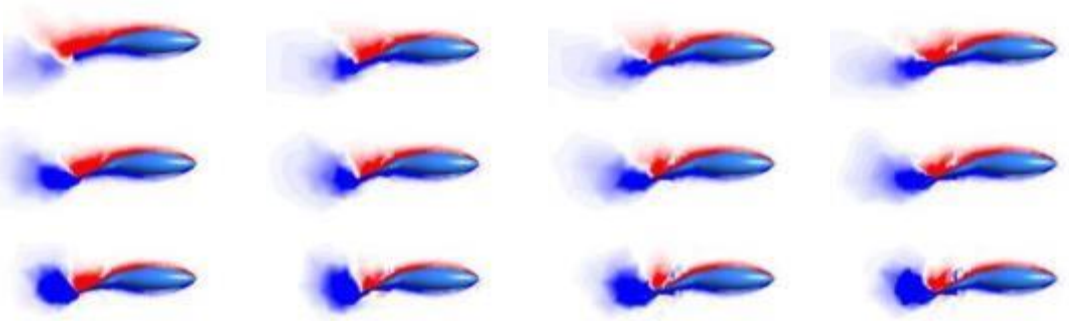			
	0.5				
	1				

(b)

Figure 5 Vorticity Y-components, |ωY| = 1 s-1, at maximum deflection: (a) variation on flow velocity, and (b) variation on tail-beat frequency. (Blue: negative vorticity, Red: positive vorticity)

By using (6), maximum efficiency at 100% can be obtained by producing thrust without lateral movement of the propulsor, P_L = 0 W. On the contrary, minimum efficiency is achieved when there is no thrust generated by the lateral movement.

The effect of the rear fin-shape in thrust generation can be observed by examining the generated vortices. In a constant mass flow, the force by the fluid is affected by its momentum change over time, specifically the change of velocity component of the fluid. The change of velocity vector in a space can be represented by its vorticity. Vorticity, $\vec{\omega}$, can be expressed as:

$$\vec{\omega} = \nabla \times \vec{v} \quad \textbf{(7)}$$

$$\vec{\omega} = \left(\frac{\partial v_z}{\partial y} - \frac{\partial v_y}{\partial z}, \frac{\partial v_x}{\partial z} - \frac{\partial v_z}{\partial x}, \frac{\partial v_y}{\partial x} - \frac{\partial v_x}{\partial y}\right) \quad \textbf{(8)}$$

III. Results and Discussion

A. *Effects of the rear fin-shapes*

There were four caudal fin models with different rear fin-shape profiles in the present simulation. The effect of the profiles on thrust production to overcome drag can be represented by the net force, F_N, and approximated cruising speed. In the condition of generated thrust is higher than drag in negative value of F_N, the model should have acceleration to move in forward direction. In case of positive F_N, oscillation parameters such as tail-beat frequency and amplitude produce drag more than thrust. Hence, at the fluid velocity higher than cruising speed of the model, the model has no ability to move forward. By using similar procedure as in previous section, cruising speed of the overall configuration can be tabulated as in Table 4.

Differences in values of parameters in Table 4 indicate that the rear fin-shapes of the oscillating fin affect the overall performance of the model. On each tail-beat frequency, cruising velocity differences are not significant between rear fin-shapes. The condition may occur due to similar fin aspect ratio, surface area, Reynolds number, and tail-beat amplitude. However, higher tail-beat frequency decreases the efficiency performance of the propulsor. The impulse thrust generator has larger growth of the efficiency reduction than vortex thrust

generator, in which round shape has the largest efficiency reduction.

The result in Table 4 indicates that impulse thrust generators should be implemented in low-speed and short-range mission. On the other side, due to lower efficiency reduction, vortex thrust generators are able to achieve higher cruising speed by increasing tail-beat frequency. Hence, longer cruising mission can be accomplished by using fork or lunate rear fin-shape. The possible applicability of the rear fin-shape based on the present simulation can be tabulated in Table 5.

The present research investigates the effect of rear fin-shape on the fin performance by considering vorticity of the flow surrounding the body and fin. Vorticity at a constant tail-beat frequency can be seen in Table 5(a). As already tabulated quantitatively in Table 4, the models have a significant different at the value of efficiency. On the figure, the efficiency can be represented qualitatively by the ratio of the area between blue and red vortices. Larger area of the blue vortices represents higher generated thrust. Table 5(b) shows vorticity at a constant flow velocity. As the higher tail-beat frequency, larger area of blue vortices is created. Hence, higher tail-beat frequency generates higher thrust. Furthermore, the ratio between blue and red vortices is higher as tail-beat frequency increases.

Table 4 Performance of the flat model configuration

Tail-beat Frequency (Hz)	Fin Shape	Cruising Speed (m/s)	Efficiency (%)
0.25	Round	0.33	64.27
	Truncate	0.33	63.29
	Fork	0.33	62.09
	Lunate	0.33	60.75
0.50	Round	0.73	61.42
	Truncate	0.72	60.59
	Fork	0.73	59.70
	Lunate	0.73	58.20
1.00	Round	2.41	44.45
	Truncate	2.27	38.49
	Fork	2.34	47.56
	Lunate	2.28	46.37

Table 5 Suitable applicability of rear fin-shape

Rear fin shape	Suitable application
Round	Maneuver, low speed, short cruising mission
Truncate	Maneuver, medium speed, medium cruising mission
Fork	Medium speed, long cruising mission
Lunate	High-speed, high endurance, long cruising mission

B. Effects of the cupping shape

Cupping shape affects the flow behaviour leaving rear part of the oscillating fin. Figure 6 shows the efffect of cupping shape on vorticity, ω_Y, for round rear fin-shape. As shown in the figure, cupping shape increase the area of the blue vorticity and decrease the area of red vorticity. The configuration indicates that cupping shape increase thrust and efficiency of the round-rear shape.

The comparison of the performance between flat and cupping shape for the overall rear fin-shapes can be seen in Figure 7. From the figure, the cupping shape increases thrust by almost twice as produced by the flat shape. Impulse thrust generator has a higher thrust increasing than vortex thrust generator. The result indicates that cupping shape is more effectively useful for shapes with extended arc shape. In the term of efficiency, cupping shape configuration on the present work reduces efficiency by the amount of 10% at medium cruising speed. However, the reduction on effciency is small compare to the increasing in thrust.

Figure 6 Vorticity-Y components, $|\omega Y| = 1\ s^{-1}$, at V = 0.5 m/s, $f = 0.5\ s^{-1}$ and θ = 20° of the round rear fin-shape: flat (left) and cupping (right)

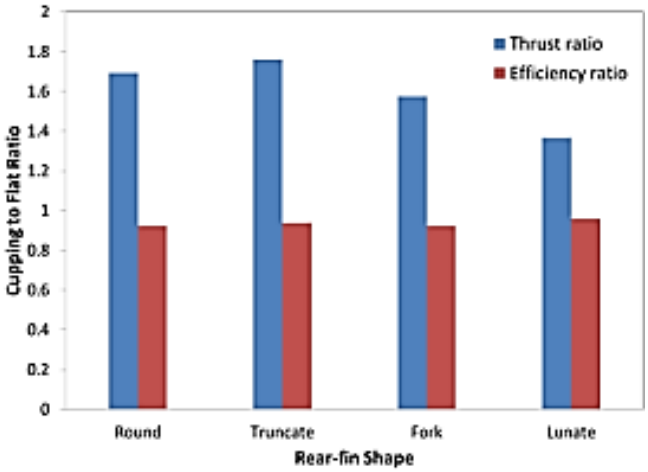

Figure 7 Effect of cupping shape on rear fin-shape performance

IV. CONCLUSIONS

Numerical simulations have been performed to observe the effect of rear fin-shape to the thrust production and efficiency of the drag-based oscillating fin models. Rear fin-shape determines the suitable mission for the models. Impulse thrust generators such as round and truncate rear fin-shapes are suitable for short cruising and maneuver mission, while vortex thrust generator such as fork and lunate rear fin-shapes are suitable for long range cruising mission. Investigation of the effect of material elasticity, which is represented by the cupping shape, shows a significant effect on thrust production at impulse thrust generators. However, by using the present cupping ratio, C_R = 0.2, at the medium speed of 1 L/s, overall efficiency performance decreases about 10%, compare to the flat configuration. Vorticity field can be a useful tool in order to describe the effect of shape and motion of the fin on thrust generation and efficiency. The preliminary study could be extended to the experimental activities in order to have validation data. The future model can be including higher degree of freedom of the fin movement, lift-based fin, and maneuvering state of the model. The importance of fin surface

deformation, such as in cupping shape, to obtain the optimum design of thrust production and efficiency could also be studied further.

ACKNOWLEDGMENT

The authors gratefully acknowledge supports of Center for Unmanned System Studies ITB (CentrUMS-ITB). The first author would also like to acknowledges support from Indonesia Endowment Fund for Education (LPDP).

REFERENCES

[1] P.W. Webb, "Simple physical principles and vertebrate aquatic locomotion," Amer. Zool., vol.28, pp. 709-725, 1988. CrossRef

[2] P.W. Webb, "Form and function in fish swimming," Scientific American, 25, 58–68, 1984. CrossRef

[3] *C.* M. Breder, " The locomotion of fishes," Zoologica, vol. 4, pp. 159-256, 1926.

[4] M.S. Triantafyllou, G.S. Triantafyllou, "An efficient swimming machine," Scienctific American, 272, 64–70, 1995. CrossRef

[5] J.M. Anderson, K. Streitlien, D.S. Barret, M.S. Triantafyllou, "Oscillating foilsd of high propulsive efficiency," J. Fluid Mech., vol. 360, pp. 41–72, 1998. CrossRef

[6] D.A. Read, F.S. Hover, M.S. Triantafyllou, "Forces on oscillating foils for propulsion and maneuvering," Journal of Fluids and Structures 17, 163–183, 2003. CrossRef

[7] H. Yamaguchi, N. Bose, "Oscillating foils for marine propulsion," Proceedings of the Fourth International Offshore and Polar Engineering Conference, 539-544, 1994.

[8] Qin Yan, Zhen Han, Shi-wu Zhang, Jie Yang, "Parametric Research of Experiments on a Carangiform Robotic Fish," Journal of Bionic Engineering 5, 95-101, 2008. CrossRef

[9] Jindong Liu and Huosheng Hu, "Biological inspiration from carangiform fish," Journal of Bionic Engineering 7, 35–48, 2010. CrossRef

[10] Daegyoum Kim and Morteza Gharib, "Characteristics of vortex formation and thrust performance in drag-based paddling propulsion," The Journal of Experimental Biology 214, 2283-2291, 2011. CrossRef

[11] C.J. Esposito, J.L. Tangorra, B.E. Flammang, G.V. Lauder, "A robotic fish caudal fin: effects of stiffness and motor program on locomotor performance," The Journal of Experimental Biology 215, 56-67, 2012. CrossRef

[12] G.V. Lauder, P.G.A. Madden, "Learning from fish: kinematics and experimental hydrodynamics for roboticist," International Journal of Automation and Computing 4, 325-335, 2006. CrossRef

[13] Zhenying Guan, Weimin Gao, Nong Gu, Saeid Nahavandi, "3D hydrodynamic analysis of a biomimetic robot fish," 11th. Int. Conf. Control, Automation, Robotics and Vision Singapore, 2010. CrossRef

[14] Iman Borazjani and Mohsen Daghooghi, "The fish tail motion forms an attached leading edge vortex," Proc. R. Soc. B 2013 280, 2013. CrossRef

[15] Stefan Kern and Petros Koumoutsakos, "Simulations of optimized anguiliform swimming," The Journal of Experimental Biology 209, 4841-4857, 2006. CrossRef

[16] Osamu Mochizuki, "Fluid dynamics on swimming animals," Proceedings of the 13th Asian Congress of Fluid Mechanics, 2010.

[17] T. Salumäe, M. Kruusmaa, "A Flexible Fin with Bio-Inspired Stiffness Profile and Geometry," Journal of Bionic Engineering 8, pp. 418–428, 2011. CrossRef

[18] Florian Menter, "Improved Two-Equation k-ω Turbulence Model for Aerodynamic Flows," NASA Technical Memorandum 103975, 1992.

[19] https://en.wikipedia.org/wiki/Bowfin

[20] https://en.wikipedia.org/wiki/Trout

[21] https://simple.wikipedia.org/wiki/Pilot_fish

[22] https://en.wikipedia.org/wiki/Crevalle_jack